ResearchGate

See discussions, stats, and author profiles for this publication at: https://www.researchgate.net/publication/231647598

Isotope Effect in the Interaction between Gas-Phase Isotopologues and Polymer-Coated Porous Silicon Over Silicon Microcantilevers

ARTICLE *in* THE JOURNAL OF PHYSICAL CHEMISTRY C · JULY 2011

Impact Factor: 4.77 · DOI: 10.1021/jp202145y

CITATIONS
3

READS
24

4 AUTHORS:

Ariel Shemesh
Technion - Israel Institute of Technology
14 PUBLICATIONS **21** CITATIONS
SEE PROFILE

S. Stolyarova
Technion - Israel Institute of Technology
67 PUBLICATIONS **298** CITATIONS
SEE PROFILE

Yael Nemirovsky
Technion - Israel Institute of Technology
261 PUBLICATIONS **3,736** CITATIONS
SEE PROFILE

Yoav Eichen
Technion - Israel Institute of Technology
108 PUBLICATIONS **3,532** CITATIONS
SEE PROFILE

Available from: Yoav Eichen
Retrieved on: 03 February 2016

THE JOURNAL OF PHYSICAL CHEMISTRY C

ARTICLE

pubs.acs.org/JPCC

Isotope Effect in the Interaction between Gas-Phase Isotopologues and Polymer-Coated Porous Silicon Over Silicon Microcantilevers

Ariel Shemesh,*,† Sara Stolyarova,‡ Yael Nemirovsky,*,‡ and Yoav Eichen*,†

†Schulich Faculty of Chemistry and ‡Department of Electrical Engineering, Technion—Israel Institute of Technology, Technion City, 32000, Haifa, Israel

ABSTRACT:

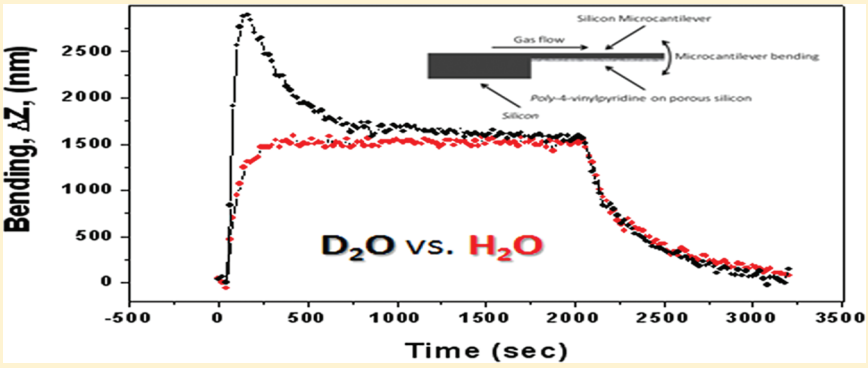

A kinetic isotope effect is observed in the guest-induced bending curves of poly-4-vinylpyridine-coated microcantilevers. Protiated (nondeuterated) and deuterated isotopologues of ethanol, water, and acetone exhibit a clear difference in their time dependent bending response patterns. While most protiated species exhibit Langmuir-type absorption bending curves, the bending curves of deuterated species are characterized by a clear overshoot. Time-dependent Fourier-transform infrared measurements provide further insight into the interrelation between molecular level interactions and macroscopic mechanical bending. A model is suggested to interpret these observations.

INTRODUCTION

Microcantilevers have gained much attention in recent years as a promising platform for biomechanical as well as chemomechanical sensors.[1−6] Different groups have reported the ability to detect different chemical substances, including explosives and warfare agents.[7,8] Microcantilever-based systems also allow label-free[6,9] real-time monitoring of chemical and biological processes such as sequence specific DNA hybridization[10] and drug-target binding interactions.[11] Recently, because of their high sensitivity, microcantilevers have been used to measure the physical properties of polymers near their glass transition temperature.[12,13]

Typically, microcantilevers can be operated in both static and dynamic modes. In the static mode, the bending (deflection) of the tip serves as a measure for the interaction between the microcantilever and the guest, while in the dynamic mode the shifts in the resonance peak indicate changes in the mass and stiffness of the microcantilever.[1,4]

In a static bending mode it is essential to asymmetrically functionalize the microcantilever so a stress gradient across it can be developed and induce bending. For example, this asymmetry can be achieved by coating one of the microcantilever surfaces with gold and using ligands that bind covalently to the gold surface through gold−thiol interactions.[14] When using polymers for coating, inkjet spotting is more common. Here, individual microdroplets are dispensed over one of the microcantilever surfaces; these droplets coalesce to form a thin polymer film. This polymer application has some drawbacks, including non uniformity in polymer thickness and the risk of contaminating the opposite surface. In addition, to achieve large microcantilever bending, the polymer needs to be relatively thick, on the scale of micrometers.[15,16]

In general, the sensitivity of a microcantilever is linked to its surface area and can be greatly enhanced by increasing it. This sensitivity enhancement has been achieved by fabricating grooves,[17] or pores[18,19] on one of the microcantilever surfaces or by using a nanoporous sensing layer.[20] Selectivity in the sensing process was achieved either by selecting a target-specific sensing layer showing higher affinity toward one substance over others[21] or by using an array of microcantilevers, each bearing a different recognition layer. By following the overall response and using mathematical discrimination methods, a specific pattern can be revealed for each of the guests.[15,22]

Despite the impressive progress made in the field, efforts are still directed toward a better understanding of the correlation

Received: March 7, 2011
Revised: June 28, 2011
Published: July 01, 2011

ACS Publications © 2011 American Chemical Society

between molecular level recognition processes and macroscopic mechanical bending phenomena.[23,24] This correlation must involve a complex interplay between many factors such as kinetics, thermodynamics, and mechanics.[25]

The difference between isotopologues is often reflected in their kinetics in performing chemical as well as physical processes. In most cases, isotopologues have also slightly different thermodynamic properties, such as vapor pressure and melting points. These stem from the differences in their mass and zero point energy. A kinetic isotope effect is the dependence of the rate of a chemical reaction on the isotopic composition of the reacting species. The kinetic isotope effect is expressed as the ratio between the rates of two given isotopologues in a reaction. Isotopic labeling, which affects the rate of a reaction, often serves as a tool for unveiling chemical mechanisms.[26,27] It is therefore surprising to note that isotopic labeling has never been used for studying host−guest interactions on microcantilevers and the way such processes induce mechanical bending phenomena.

Recently, we reported on the kinetic isotope effect in the interaction between ethanol and water gas-phase isotopologues and poly-4-vinylpyridine-(P4VP)-coated asymmetric porous-silicon-oversilicon (PSOS) microcantilevers.[28] The time dependent bending patterns of the P4VP-coated microcantilevers show considerable H/D isotope effects.

Herein, we extend this research and measure these interactions for acetone and benzene isotopologues. In addition, we present a simple kinetic chemomechanical model that is based on the interplay between stress buildup and relaxation in order to explain these observations. We present time-resolved FTIR measurements that support this model.

The P4VP is a glassy polymer at room temperature and was shown to be useful as a selective sensing layer for nitro aromatics.[29] Because of its glassy character it follows non-Fickian sorption kinetics characterized by time dependent structural rearrangement and relaxation-transport control.[30] Absorption of guest molecules causes a decrease in polymer stiffness due to segmental plasticization and develops internal stress gradients. The rate of plasticization and relaxation depends on the guest−polymer interaction, concentration of the guest and the temperature.[31]

Novel asymmetric PSOS microcantilevers made according to Figure 1, using vapor-phase stain etching,[19] offer inherently asymmetric, highly sensitive, and easy-to-coat systems. The resulting microcantilevers are characterized by a rough surface on their lower side and an intact flat surface on their upper side, Figure 2. The process which leaves the upper side intact preserves the silicon reflectivity, which is important for optical readout schemes.

Rough structures, such as the ones presented in Figure 2c, were shown to enhance the microcantilever response to adsorption of molecules because micro- and nanostructured interfaces and coatings facilitate efficient conversion of chemical interactions into mechanical bending.[1] Recent studies demonstrate an increase of up to 2 orders of magnitude in the response of the microcantilever when receptor molecules are immobilized on nano structures instead of on smooth interfaces. The enhancement originates from the fact that these structures increase the density of the binding sites.[32] Moreover, when the binding sites have three-dimensional features, adsorption induces stress through additional mechanisms including steric, osmotic, hydration, and electrostatic forces.[1] The interaction between target molecules and their surface-bound binding sites that are confined in pores also affects the

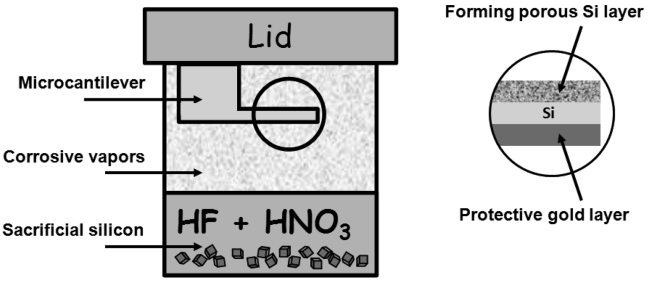

Figure 1. Vapor-phase stain etching fabrication of the PSOS layer on the lower unmasked side of the microcantilevers.

diffusion and cluster formation within the pores.[27] Furthermore, due to the enhanced chemomechanical conversion of confined polymers inside pores, thin polymer films are in most cases sufficient, in contrast to applying a polymer on smooth surfaces where thick layers are mandatory for good bending response.[16]

Therefore, PSOS microcantilevers may be efficiently derivatized with polymer layers simply by dipping them into the polymer solution and rinsing. Dipping the microcantilever chips in the polymer solution will result with a thin and homogeneous polymer film. The polymer layer atop the porous side of the PSOS microcantilever is the dominant one in generating guest-induced stress, mainly due to its high surface area.

EXPERIMENTAL SECTION

Asymmetrization of Microcantilevers. Commercial microcantilever arrays (Octensis, Micromotive GmbH, Mainz, Germany) with dimensions of 500 μm long, 90 μm wide, and 1 μm thick were asymmetrized prior to polymer coating. The asymmetrization was achieved by the deposition of 50 nm gold as a protective mask atop one of the microcantilevers faces and then fabrication of a porous silicon layer on the opposite face, using reaction induced vapor-phase stain etching, Figure 1.

The microcantilever arrays were mounted on a holder above a vessel containing HNO_3 (40 mL, 65%) and HF (10 mL, 49%). Silicon powder (100 mg) was added to the acid mixture, serving as a catalyst. After etching, the array was removed from the reaction vessel and rinsed in distilled water. The protective gold mask was removed using KI:I_2:H_2O (4:1:40 w/w), and the microcantilever arrays were then rinsed in distilled water. The resulting microcantilever arrays were characterized by the PSOS layer on the unmasked (lower) side and an intact flat native oxide over silicon on the masked (upper) side.

Polymer Coating of Asymmetrized Microcantilevers. P4VP (10 mg, Sigma-Aldrich, $M_w \approx 160{,}000$) was dissolved in dimethylformamide (DMF, 100 mL). The microcantilever array was immersed into the polymer solution for 15 min and then pulled out of solution and dipped three times in pure DMF for 20 s to obtain a thin, homogeneous, and uniform polymer layer.

Figure 2a depicts scanning electron microscopy (SEM) micrographs of a representative microcantilever array after asymmetrization and coating. Parts b and c of Figure 2 depict SEM micrographs of the upper (b) and lower (c) surfaces of the microcantilever. While the gold masked face retained its flat intact surface (Figure 2a), the face that was exposed to the vapor stain etching process turned rugged and porous (Figure 2c).

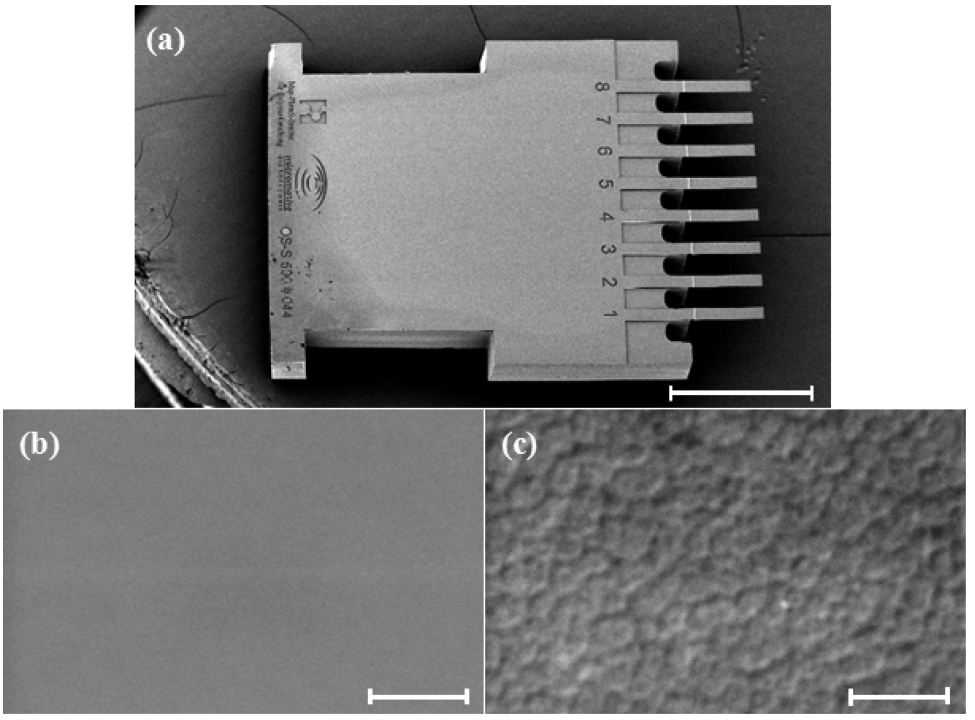

Figure 2. (a) A SEM micrograph of a microcantilever array used in this study as the transducer. Representative SEM images of the upper (masked, b) and lower (unmasked, c) surfaces of the polymer coated microcantilever depicted in a. Bar size: 1 mm in part a and 5 μm in parts b and c.

Instruments. SEM images were taken using a Phillips XL 20 scanning electron microscope. The guest molecules H_2O, benzene, acetone, ethanol (BioLab), CH_3CH_2OD, CD_3CD_2OD, D_2O, benzene-d_6, and acetone-d_6 (all the materials used in this work were purchased from Sigma-Aldrich unless otherwise noted) were used as received. Figure 3 shows a scheme of the apparatus used for performing the different microcantilever bending experiments. The microcantilever array was held in a temperature controlled flow cell. All experiments were performed at 303 ± 0.5 K and at a flow rate of 100 ± 2 mL/min, unless otherwise noted. To fix the vaporizing surface of the liquid guests, they were placed in the guest chamber in a glass cuvette having an internal diameter of ϕ_{id} = 10 mm. The bending of the microcantilevers was measured through a window at the top of the flow cell using an optical profiling measurement system (NT1100, Veeco). The tip height was measured with respect to a reference surface using dedicated software (SureVision).

FTIR measurements (Tensor 27, Bruker optics) were performed on a polymer sample held in a stainless steel gas-tight flow cell equipped with two KBr windows on its opposing faces. A gas flow system similar to the one depicted in Figure 3 was used. P4VP was drop-cast from solution on one of the KBr windows. Experiments were performed at room temperature.

RESULTS AND DISCUSSION

The Effect of Isotope Substitution on Bending. P4VP, **1**, coated PSOS microcantilevers were placed in a temperature controlled constant flow cell with a flow rate of 100 ± 2 mL min^{-1} of the carrier gas (N_2), Figure 3. The bending of the microcantilevers was measured using an optical profiling system as a function of the time in the presence and absence of guest molecules (Figure 4) in the carrier gas.

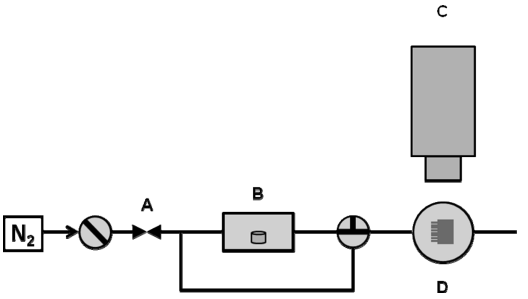

Figure 3. Schematic drawing of the apparatus used for performing the different microcantilever bending experiments. A, flow meter; B, guest evaporation chamber with guest container; C, optical profiling system; D, temperature-controlled flow cell with an optical window.

Figure 5 depicts representative guest-induced P4VP, **1**, coated PSOS microcantilever bending curves in the presence of three ethanol isotopologues, CH_3CH_2OH, **2**, CH_3CH_2OD, **3**, and CD_3CD_2OD, **4**, as the guests. With the aim of reducing measurement and production errors and variations, all experiments were run on the same microcantilever array without moving/removing it between experiments. The same results were reproduced on numerous arrays.

The bending curves reflect the strong, micrometer scale, response of the PSOS microcantilevers, originating from a polymer layer (approximately 100 nm thick, measured by TOF-SIMS surface analysis) residing in the porous silicon matrix. A detailed study on the fabrication and characterization of PSOS microcantilevers will be discussed in a dedicated paper.

From Figure 5 it is evident that in all cases the interaction between the guest molecules and the polymer coated PSOS results with an upward bending, away from the dominant

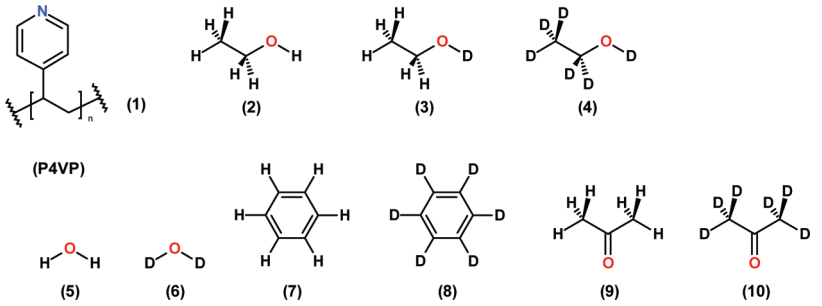

Figure 4. P4VP, **1**, and the guest molecules used in the different experiments.

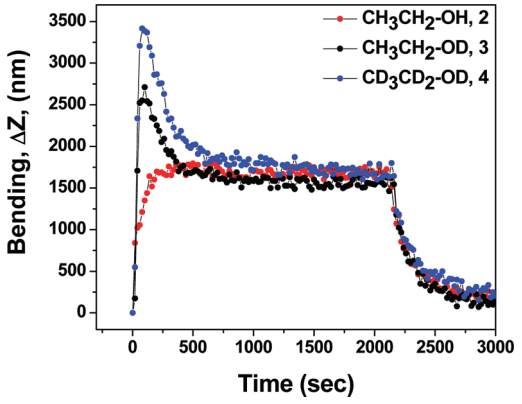

Figure 5. Guest-induced microcantilever bending curves of a P4VP, **1**, coated PSOS microcantilever in the presence of three ethanol isotopologues, CH_3CH_2OH, **2**, (red), CH_3CH_2OD, **3**, (black), and CD_3CD_2-OD, **4**, (blue) as the guests. N_2 as the carrier gas, 100 mL/min, T = 303 ± 0.5 K.

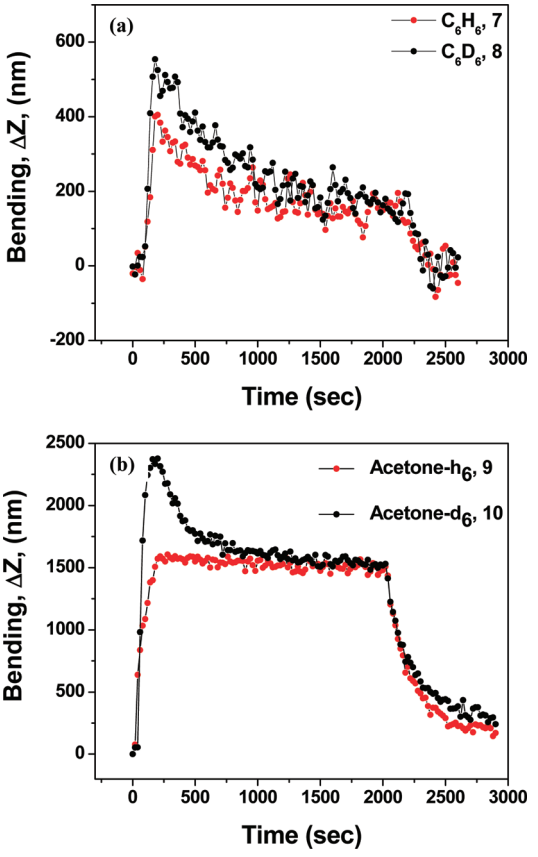

Figure 6. Guest-induced microcantilever bending curve of a P4VP, **1**, coated PSOS microcantilever in the presence of (a) benzene, **7**, (red), and deuterated benzene, **8**, (black) and (b) acetone, **9**, (red), and deuterated acetone, **10**, (black) as the guests. N_2 as the carrier gas, 100 mL/min, T = 303 ± 0.5 K.

polymer film on the lower porous side of the microcantilever.[33] As the interaction between ethanol isotopologues and P4VP results in swelling of the polymer, this is a clear indication that the dominant effect originates from the polymer residing on the porous side of the microcantilever. Additionally, while the protiated ethanol isotopologue, **2**, exhibits a typical Langmuir-type adsorption curve, the curves of the two deuterated isotopologues **3** and **4** are characterized by a bending overshoot, followed by relaxation to a steady-state value that is practically identical for all three ethanol isotopologues. The bending curves of the deuterated ethanol isotopologues **3** and **4** also differ from one another, with the fully deuterated isotopologue **4** having a larger overshoot. Upon turning off the flux of the guest molecules (keeping the stream of nitrogen constant) the guest desorbs from the polymer-coated microcantilever, inducing its relaxation into its original baseline. This process follows a first exponent with a practically identical decay time constant of τ = 175 ± 10 s for the different isotopologues.

Isotope effect on the guest-induced microcantilever bending is not limited to ethanol. The time-dependent guest-induced microcantilever bending curves of a typical P4VP, **1**, coated PSOS microcantilever in the presence of protiated and deuterated isotopologues of benzene, **7**, **8**, acetone, **9**, **10**, water, **5**, **6**, are shown in Figures 6a, 6b, and 7a, respectively.

As can be seen from Figure 6, the characteristic overshoot in the time dependent guest-induced microcantilever bending curves has different height and relaxation time, depending on the deuterated species. For example, Figure 6a shows the response of the microcantilevers to benzene, **7**, and its deuterated analogue benzene-d_6, **8**. Both isotopologues of benzene induce rather small bending responses with similar steady states. Here, overshoot characterizes both benzene isotopologues, but still higher overshoot is observed for the deuterated analogue. On the other hand, Figures 6b and 7a depict pronounced response for acetone and water, respectively. One would expect that isotope substitution at the hydroxyl groups, such as in ethanol and water, would give rise to large isotope effects in terms of overshoot height and time of relaxation. Nevertheless, as can be clearly seen in Figures 5 and 6, deuteration of methyl groups seems to

dx.doi.org/10.1021/jp202145y |J. Phys. Chem. C 2011, 115, 15980–15987

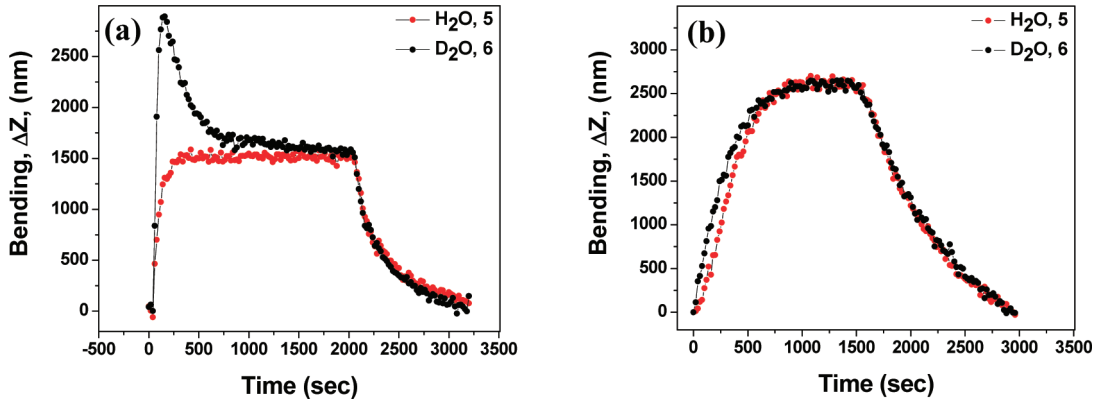

Figure 7. Flow-rate dependency of guest-induced microcantilever bending curves of a P4VP, **1**, coated PSOS microcantilever in the presence of H_2O, **5**, (red) and D_2O, **6**, (black) as the guests, with N_2 as the carrier gas. (a) 100 mL/min, (b) 20 mL/min, $T = 303 \pm 0.5$ K.

contribute significantly to the difference in the bending response as well, implying that at least part of the effect is associated with a secondary isotope effects.[26] Secondary isotope effects were reported for different reactions[26] but were also found to be associated with host−guest processes.[34] Isotope effects on solvation dynamics were observed for methanol, showing that deuterium substitution increased the solvation time. Most effective was the deuteration at the hydroxyl groups which increased the average solvation time by ∼10% while deuteration at the methyl groups had only a ∼5% increase. Furthermore, deuteration of each group was found to be additive on the overall solvation time, similar to what can be seen in Figure 5.[35]

Interestingly, the appearance of a bending overshoot depends on the flow rate. For example, Figure 7 compares the time dependent bending of the microcantilever at different flow rates of D_2O and H_2O vapors. As can be clearly seen, at a flow rate of 100 mL/min, Figure 7a, the bending overshoot is clearly visible for D_2O while absent for H_2O. At a flow rate of 20 mL/min, Figure 7b, the bending overshoot disappears, and the two guests look practically the same, with a modest difference at the pre-steady-state part of the curve.

In general, an overshoot is observed whenever the system consists of at least two consecutive processes of buildup and decay, of which the earlier step is faster than the later one ($\tau_1 < \tau_2$).[24] As the rate of absorption depends on the flux of the guest vapors (and thus on the flow rate) switching from a high flow rate (100 mL/min in our case) to a low flow rate (20 mL/min in our case) is expected to balance the system between a set of conditions that allow the formation of a bending overshoot ($\tau_1 < \tau_2$) to a set of conditions that do not allow for the formation of a bending overshoot ($\tau_1 \geq \tau_2$).

The steady-state bending observed in parts a and b of Figure 7 is different, being larger at the low flow rate. This difference originates from the differences in steady-state concentrations of the guest in the carrier gas, being ∼1:1.5 for 100 and 20 mL/min, respectively (FTIR).

Time-Resolved FTIR Measurements. In an attempt to gain further information on the molecular scale events taking place in the system and study the supramolecular interactions between the guest and the polymer, time-resolved FTIR measurements were carried out. The interaction between a film of P4VP and the two isotopologues of water, H_2O, **5**, and D_2O, **6**, was studied by following the infrared spectrum of the system, especially the relevant absorbance peaks of the −OH and −OD species, centered at ∼3200 and

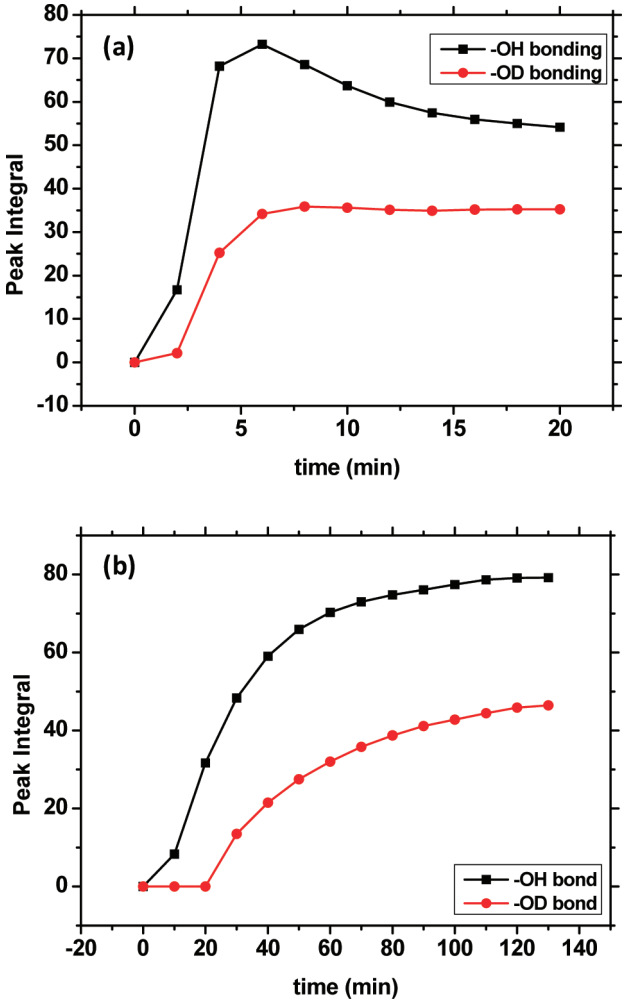

Figure 8. Time-resolved FTIR measurements showing the area under the −OH/−OD absorption peaks for a film of P4VP, **1**, under H_2O, **5**, (black), and D_2O, **6**, (red) atmospheres. N_2 served as the carrier gas at RT. (a) 100 mL/min, (b) 20 mL/min.

∼2600 cm^{-1}, respectively, as a function of the time. In both cases, the steady-state concentrations of the two isotopologues in the polymer matrix are about the same at both flow rate regimes, based on the analysis of the areas under the peaks.[36] Figure 8 presents the

dx.doi.org/10.1021/jp202145y |J. Phys. Chem. C 2011, 115, 15980–15987

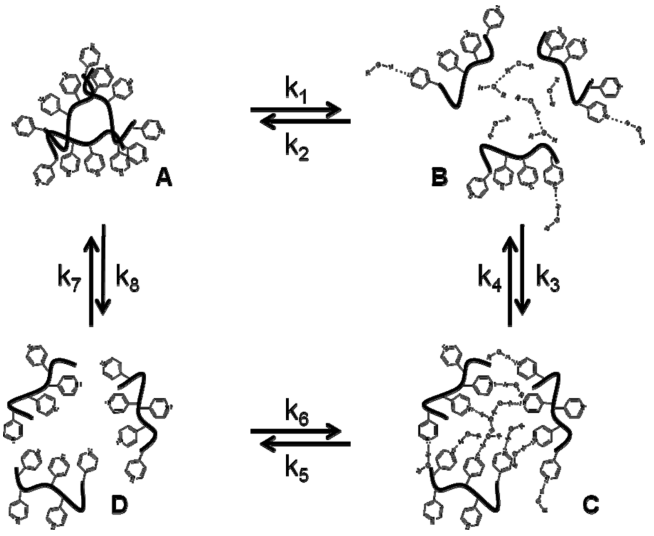

Figure 9. Proposed model for the P4VP, **1**, coated PSOS microcantilever−guest interaction. The model incorporates 4 different states and k_{1-8} stand for kinetic rate constants. State A, the polymer host prior to guest exposure; state B, unrelaxed host−guest complex; state C, relaxed host−guest complex; state D, polymer host after desorption of guest, unrelaxed.

time dependent buildup curves of the −OH and −OD absorption peaks at the high and low flow rate regimes.

At the high flow rate (100 mL/min), the area under the peaks of both the −OH and −OD absorption bands is characterized by a small delay, being somewhat larger for the −OD peaks. The buildup times of the −OH and −OD peaks look very different where the −OH peak builds up faster than that of the −OD. Furthermore, the buildup of the −OH absorption is characterized by an overshoot, meaning that the area under the peak increases then decreases upon reaching steady-state conditions. This behavior is in marked contrast to the behavior of the −OD peak that smoothly reaches equilibrium without passing through an overshoot.

At the lower flow regime (20 mL/min) the −OH peak still builds up faster than that of the −OD, which shows even longer delay at buildup. No overshoot is observed for any of the species at this flow regime, Figure 8b.

Time-resolved FTIR measurements clearly show that the protiated guest species are faster than their deuterated analogs in forming polymer bound complexes. This is observed both at the high and low flow rate regimes. In accordance with our observations on the gas flow-rate dependent microcantilever bending (see Figure 7), one can clearly see a difference in the steady-state −OH and −OD IR peaks where at the low flow rate regime (20 mL/min) the peaks are ca. 1.5 times larger than the same peaks at the high flow rate regime (100 mL/min). We attribute this difference in the peak intensity to the difference in the concentrations of the vapors of the guests in the nitrogen atmosphere. The concentration of the guest molecules in the nitrogen carrier gas depends on the contact time the nitrogen flow has with the evaporating guest in the guest evaporation chamber (Figure 3). Consequently, in the fast flowing nitrogen stream the concentration of the guests is smaller than in the slow flowing nitrogen stream.

Model. Guest-induced microcantilever bending shows different behaviors for protiated and deuterated guest analogues. In all cases, the difference is expressed at the pre-steady-state stage, mostly in the form of an overshoot for the deuterated species, while at steady-state the differences in bending are negligible. This isotope dependent behavior could also be reproduced in the time-dependent FTIR study of the interaction between films and the water isotopologues. The overshoot phenomenon describes an event where the observed quantity or signal exceeds its steady-state value. This phenomenon is well documented in the literature for many different systems spanning from control, biology, and polymer systems in solutions of different pH values.[37−39] In general, such behavior is observed whenever the system consists of at least two consecutive processes of buildup and decay. Yet, another prerequisite for the appearance of such an overshoot is that the earlier step is faster than the later one.

Apparently, in our case, the arrival to steady-state under constant flow of the guest must involve at least two processes, one being the absorption of the guest molecules to the host and buildup of stress, while the other involves structural reorganization and relaxation of the host−guest complex and its associated relief of stress. To explain the observed overshoot and isotope effect, we propose a simplified model, outlined in Figure 9. This model ties the molecular level microscopic events with the observed macroscopic microcantilever-bending phenomena, unveiling the way molecular processes are translated into mechanical motion.

We suggest the following model in order to account for the observations presented in this manuscript.

Before exposure to the guest molecules, the guest-free P4VP polymer residing atop the microcantilever exists in an energy minimized structure, state **A** in Figure 9. Upon exposing the polymer-coated microcantilever to a flow of guest molecules in a carrier gas, two molecular level processes are expected to take place. First, absorption of the guest molecules into the host polymer (**A**→**B** in Figure 9) is driven both by entropy and enthalpy (H bonding and other weak interactions). This process is associated with a stress buildup as the polymer needs to reorganize around the guest molecules. In a second step, as the polymer−guest complex is a different entity than the polymer itself, it is expected to reorganize and relax into its own thermodynamically preferred structure, (**B**→**C** in Figure 9). This relaxation process involves both the polymer and the guest molecules and therefore may be isotope dependent. Upon removing the guest molecules from the carrier gas, desorption of the guest from the polymer−guest complex occurs (**C**→**D** in Figure 9). The desorbed state **D** consists of the free polymer in the structure it adopted in the polymer−guest complex and is thus unstable. It therefore reverts to its energy minimized structure **A** (**D**→**A** in Figure 9). This process cannot show any difference between the isotopologues since no guest exists in the system. The transition between states **C** and **A** does not necessarily require two distinct steps. In cases where the desorption of the guest is slow relative to the polymer reorganization process state **D** will not exist. In such cases an isotope effect may be observed.

In cases where **A**→**B** is equal to or slower than **B**→**C** the rate determining step is **A**→**B** and no residual buildup of stress occurs as the polymer−guest complex reorganizes faster than it is formed. In such cases any physical property of the polymer−guest complex will change in a smooth manner without showing an overshoot. In contrast, in cases where **A**→**B** is faster than **B**→**C** the rate determining step is **B**→**C** and the residual buildup

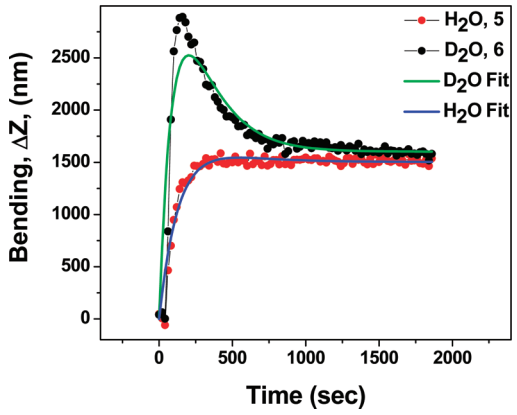

Figure 10. Experimental guest-induced microcantilever bending curves for H_2O, **5**, (red) and D_2O, **6**, (black) and best-fit curves for H_2O, **5** (blue) and D_2O, **6** (green) according to eq 2.

of stress must occur as the polymer−guest complex reorganizes slower than it is formed. This residual stress will be relieved by structural reorganization and subsequent relaxation of the polymer−guest complex at a later time when the **A**→**B** is about to complete because of saturation of the guest binding sites in the polymer. In such systems any physical property of the polymer−guest complex that follows the guest absorption process is expected to exhibit an overshoot.[24,40]

As was shown in Figure 8, FTIR measurements clearly show that the rate build up of the polymer−guest complex is faster for H_2O, **5**, than for its deuterated isotopologue, D_2O, **6**, at both the high and low flow rate regimes. Therefore, one may assume that the ability of the protiated-polymer complex to relax is faster than that of the deuterated-polymer complex.

The relief of the stress through structural reorganization and relaxation is normally associated with the macroscopic property of polymer Young's modulus.[41] The ability of polymers to relax upon binding a guest through structural reorganization is directly related to polymer-chain mobility. Thus, the reorganization−relaxation process depends on the nature of the polymer. Because of the high mobility of their chains, rubberlike polymers attain steady state rapidly after hosting guest molecules. In contrast, glassy polymers, such as P4VP (T_g = 142 °C), are characterized by longer reorganization times.[42] Moreover, the rate of reorganization−relaxation of the polymer−guest complex is also associated with the diffusion of the guest in the polymer host. In our research, the kinetic isotope effect may be linked to the higher viscosity of deuterated guests compared to their protiated analogues.[31,43,44]

We are not the first to address the issue of overshooting microcantilever bending. In a pioneering work Heinrich, Wenzel, Josse, and co-workers modeled time dependent bending of a microcantilever carrying on it a viscoelastic layer and exposed to a constant concentration of a guest molecule.[40,24] This group developed an analytical solution for the time-dependent bending of such microcantilevers. The normalized first order approximation of their equation for the time dependent microcantilever bending is presented in eq 1, where normalized time, $\bar{t}$ is given by $\bar{t} = t/\tau_R$; τ_R being the relaxation time constant of the viscoelastic medium; $\bar{\tau}$ is the ratio between the time-dependent strain constant, τ_ε, and τ_R: $\bar{\tau} = \tau_\varepsilon/\tau_R$, β is the ratio of the thickness of the viscoelastic medium and microcantilever, ε^*_∞ is the strain at steady state, $\bar{M}_\infty$ is the normalized Young's modulus at steady state, and $\bar{\zeta}$ is given by $\bar{\zeta} = \bar{M}_0[(1-(\bar{M}_\infty/\bar{M}_0)\bar{\tau})/(1-\bar{\tau})]$, where $\bar{M}_0$ is the normalized Young's modulus of the viscoelastic medium at start.

$$\bar{w}(\bar{t}) \approx 6\beta\varepsilon^*_\infty[\bar{M}_\infty(1-e^{-\bar{t}}) + \bar{\zeta}(e^{-\bar{t}} - e^{-\bar{t}/\bar{\tau}})] \quad (1)$$

Equation 2 presents the time-dependent dimensional tip bending of the microcantilever according to eq 1 where h is the thickness of the microcantilever.

$$\Delta Z(t) = \frac{L^2\bar{w}}{2h} \quad (2)$$

This analytical treatment takes into account physical parameters of the microcantilever and its coating and defines the time constants associated with the temporal development of strain and relaxation. The group presented a simple criterion for the development of an overshoot behavior out of a monotonic (Langmuir-type) behavior relying on $\bar{\tau}$ and $(\bar{M}_0/\bar{M}_\infty)$, eq 3.

$$\vartheta \equiv \frac{\bar{M}_0}{\bar{\tau}\,\bar{M}_\infty} \quad (3)$$

According to this criterion when ϑ is unity the system is on the border between monotonic behavior and overshoot. The magnitude of the overshoot depends on the size of ϑ.

With the aim of extracting first quantitative information from our system we tried fitting the equation to our data on the time-dependent bending buildup in the case of H_2O and D_2O, Figure 10. The development of the strain had time constants, τ_ε, of 283 and 102 s for H_2O and D_2O, respectively, while the relaxation time constants, τ_R, were 133 and 210 s for H_2O and D_2O, respectively, and are in-line with our phenomenological model. Additionally, the overshoot criterion, ϑ, produced values of 1.16 and 5.14 for H_2O and D_2O, respectively, denoting practically no overshoot for H_2O and a strong overshoot for D_2O.

While the use of the Heinrich, Wenzel, and Josse model clearly provides insight into our system, it is clear that further work needs to be done in order to correlate molecular level interactions and processes with macroscopic mechanical phenomena.

CONCLUSIONS

Time-dependent guest-induced microcantilever bending curves of P4VP, **1**, coated PSOS microcantilevers show a kinetic isotope effect with various gas phase guests. In contrast, the steady-state bending of the different guests is practically independent of the isotopologue.

FTIR measurements show a similar kinetic isotope effect and absence of any significant steady-state isotope effect. A model is suggested to account for the isotope effect in the time dependent microcantilever bending. The model considers kinetic factors affecting the bending behavior. The isotope effect on the bending curves of the microcantilever is explained in terms of molecular scale interactions and processes. First quantitative data was obtained using the Heinrich, Wenzel, and Josse model for time dependent microcantilever bending, showing the difference in stain buildup and relaxation between H_2O and D_2O.

AUTHOR INFORMATION

Corresponding Author

*E-mail: arielshe@tx.technion.ac.il (A.S.); nemirov@ee.technion.ac.il (Y.N.); chryoav@tx.technion.ac.il (Y.E.).

■ ACKNOWLEDGMENT

This work was supported by the Technion Funds for Security Research. In addition, a contribution of the KAMEA program of the Israeli Ministry of Absorption is gratefully acknowledged.

■ REFERENCES

(1) Lavrik, N. V.; Sepaniak, M. J.; Datskos, P. G. *Rev. Sci. Instrum.* **2004**, *75*, 2229–2253.
(2) Then, D.; Ziegler, C. In *Encyclopedia of Nanoscience and Nanotechnology*; Nalwa, H. S., Ed.; American Scientific Publishers: CA, 2004; pp 499−516.
(3) Grate, J. W. *Chem. Rev.* **2008**, *108*, 726–745.
(4) Raiteri, R.; Grattarola, M.; Butt, H. J.; Skladal, P. *Sens. Actuators B* **2001**, *79*, 115–126.
(5) Nemirovsky, Y.; Shemesh, A.; Stolyarova, S. *Proc. SPIE* **2008**, *6993*, 699302.1–699302.12.
(6) Yue, M.; Stachowiak, J. C.; Lin, H.; Datar, R.; Cote, R.; Majumdar, A. *Nano Lett.* **2008**, *8*, 520–524.
(7) Pinnaduwage, L. A.; Ji, H. F.; Thundat, T. *IEEE Sens. J.* **2005**, *5*, 774–785.
(8) Stolyarova, S.; Shemesh, A.; Aharon, O.; Cohen, O.; Gal, L.; Eichen, Y.; Nemirovsky, Y. *NATO Science for Peace and Security Series B: Physics and Biophysics* **2010**, 261–274.
(9) Raorane, D. A.; Lim, M. D.; Chen, F. F.; Craik, C. S.; Majumdar, A. *Nano Lett.* **2008**, *8*, 2968–2974.
(10) Wu, G. H.; Ji, H. F.; Hansen, K.; Thundat, T.; Datar, R.; Cote, R.; Hagan, M. F.; Chakraborty, A. K.; Majumdar, A. *Proc. Natl. Acad. Sci. U.S.A.* **2001**, *98*, 1560–1564.
(11) Ndieyira, J. W.; Watari, M.; Barrera, A. D.; Zhou, D.; Vogtli, M.; Batchelor, M.; Cooper, M. A.; Strunz, T.; Horton, M. A.; Abell, C.; Rayment, T.; Aeppli, G.; Mckendry, R. A. *Nature Nanotechnol* **2008**, *3*, 691–696.
(12) Jung, N.; Seo, H.; Lee, D.; Ryo, C. Y.; Jeon, S. *Macromolecules* **2008**, *41*, 6873–6875.
(13) Jung, N.; Jeon, S. *Macromolecules* **2008**, *41*, 9819–9822.
(14) Berger, R.; Delamarche, E.; Lang, H. P.; Gerber, C.; Gimzewski, J. K.; Meyer, E.; Guntherodt, H.-J. *Science* **1997**, *276*, 2021–2024.
(15) Peter, L. H.; Christoph, G. In *STM and AFM Studies on (Bio)molecular Systems: Unravelling the Nanoworld*; Springer-Verlag: Berlin, 2008, pp 1−28.
(16) Privorotskaya, N. L.; King, W. P. *Microsyst. Technol.* **2009**, *15*, 333–340.
(17) Headrick, J. J.; Sepaniak, M. J.; Lavrik, N. V.; Datskos, P. G. *Ultramicroscopy* **2003**, *97*, 417–424.
(18) Fernandez, R. E.; Stolyarova, S.; Chadha, A.; Bhattacharya, E.; Nemirovsky, Y. *IEEE Sensors* **2009**, *9*, 1660–1666.
(19) Stolyarova, S.; Cherian, S.; Raiteri, R.; Zeravik, J.; Skladal, P.; Nemirovsky, Y. *Sens. Actuators B* **2008**, *131*, 509–515.
(20) Datskos, P. G.; Lavrik, N. V.; Sepaniak, M. J. *Sens. Lett.* **2003**, *1*, 25–32.
(21) Raiteri, R.; Nelles, G.; Butt, H. J.; Knoll, W.; Skladal, P. *Sens. Actuators B* **1999**, *61*, 213–217.
(22) Baller, M. K.; Lang, H. P.; Fritz, J.; Gerber, C.; Gimzewski, J. K.; Drechsler, U.; Rothuizen, H.; Despont, M.; Vettiger, P.; Battiston, F. M.; Ramseyer, J. P.; Fornaro, P.; Meyer, E.; Guntherodt, H. J. *Ultramicroscopy* **2000**, *82*, 1–9.
(23) Watari, M.; Galbraith, J.; Lang, H. P.; Sousa, M.; Hegner, M.; Gerber, C.; Horton, M. A.; McKendry, R. A. *J. Am. Chem. Soc.* **2007**, *129*, 601–609.
(24) Wenzel, M. J.; Josse, F.; Heinrich, S. M.; Yaz, E.; Datskos, P. G. *J. Appl. Phys.* **2008**, *103*, 064913−1–11.
(25) Sushko, M. L.; Harding, J. H.; Shluger, A. L.; McKendry, R. A.; Watari, M. *Adv. Mater.* **2008**, *20*, 3848–3853.
(26) Kohen, A.; Limbach, H. H. *Isotope Effects in Chemistry and Biology*; Taylor & Francis: New York, 2006.
(27) Fletcher, A. J.; Thomas, K. M. *J. Phys. Chem. C* **2007**, *111*, 2107–2115.
(28) Shemesh, A.; Stolyarova, S.; Nemirovsky, Y.; Eichen, E. *J. Mater. Chem.* **2011**, *21*, 2070–2073.
(29) Tenhaeff, W. E.; McIntosh, L. D.; Gleason, K. K. *Adv. Funct. Mater.* **2010**, *20*, 1144–1151.
(30) Sfirakis, A.; Rogers, C. E. *Polym. Eng. Sci.* **1981**, *21*, 542–547.
(31) Windle, A. H. In *Polymer Permeability*; Elsevier Applied Science Publishers: New York, 1985; Chapter 3.
(32) Lavrik, N. V.; Tipple, C. A.; Sepaniak, M. J.; Datskos, P. G. *Biomed. Microdev.* **2001**, *3*, 35–44.
(33) Bumbu, G. G.; Wolkenhauer, M.; Kircher, G.; Gutmann, J. S.; Berger, R. *Langmuir* **2007**, *23*, 2203–2207.
(34) Mugridge, J. S.; Bergman, R. G.; Raymond, K. N. *J. Am. Chem. Soc.* **2010**, *132*, 1182–1183.
(35) Shirota, H.; Pal, H.; Tominaga, K.; Yoshihara, K. *J. Phys. Chem.* **1996**, *100*, 14575–14577.
(36) Singh, S. *J. Mol. Struct.* **1985**, *127*, 203–208.
(37) Westphal, L. C. *Handbook of Control Systems Engineering*; Kluwer Academic Publishers: MA, 2001.
(38) Ohshima, H.; Baiju, H.; Hyono, A. *Colloids Surf., B* **2004**, *39*, 53–56.
(39) Díez-Pena, E.; Quijada-Garrido, I.; Barrales-Rienda, J. M. *Macromolecules* **2003**, *36*, 2475–2483.
(40) Heinrich, S. M.; Wenzel, M. J.; Josse, F.; Dufour, I. *J. Appl. Phys.* **2009**, *105*, 124903.
(41) Senturia, S. D. *Microsystem Design*; Kluwer Academic Publishers: MA, 2001; Chapter 8.
(42) Thomas, N. L.; Windle, A. H. *Polymer* **1981**, *22*, 627–639.
(43) Hakem, I. F.; Boussaid, A.; Benchouk-Taleb, H.; Bockstaller, M. R. *J. Chem. Phys.* **2007**, *127*, 224106−1–10.
(44) Soper, A. K.; Benmore, C. J. *Phys. Rev. Lett.* **2008**, *101*, 065502−1–4.